CORA Cork Open Research Archive
Cartlann Taighde Oscailte Chorcaí

Title	A 2-legged XY parallel flexure motion stage with minimised parasitic rotation
Authors	Hao, Guangbo
Publication date	2014-03-01
Original Citation	Guangbo Hao (2014) 'A 2-legged XY parallel flexure motion stage with minimised parasitic rotation'. Proceedings of the Institution of Mechanical Engineers, Part C: Journal of Mechanical Engineering Science, .
Type of publication	Article (peer-reviewed)
Link to publisher's version	http://pic.sagepub.com/content/early/2014/03/07/0954406214526865.full.pdf+html - 10.1177/0954406214526865http://online.sagepub.com
Rights	© 2014, Guangbo Hao.
Download date	2026-10-13 15:48:34
Item downloaded from	https://hdl.handle.net/10468/1527

UCC
University College Cork, Ireland
Coláiste na hOllscoile Corcaigh

A 2-legged XY parallel flexure motion stage with minimised parasitic rotation

Guangbo Hao
School of Engineering, University College Cork, Cork, Ireland
Email: G.Hao@ucc.ie

ABSTRACT: XY compliant parallel manipulators (CPMs) have been used as diverse applications such as AFM (atomic force microscope) scanners due to their proved advantages such as eliminated backlash, reduced friction, reduced number of parts and monolithic configuration. This paper presents an innovative approach of stiffness center based to design a decoupled 2-legged XY CPM in order to better minimise the inherent parasitic rotation and have a more compact configuration. This innovative design approach makes all the stiffness centers, associated with the passive prismatic (P) modules, overlap at a point that all the applied input forces can go through. A monolithic compact and decoupled XY CPM with minimised parasitic rotation is then proposed using the proposed design approach based on a 2-PP kinematically decoupled translational parallel manipulator. Its load-displacement and motion range equations are derived, and geometrical parameters are determined for a specified motion range. FEA comparisons are also implemented to verify the analytical models with analysis of the performance characteristics including primary stiffness, cross-axis coupling, parasitic rotation, input and output motion difference and actuator non-isolation effect. Compared with the existing XY CPMs obtained using four-legged mirror-symmetric constraint arrangement, the proposed XY CPM based on stiffness center approach mainly benefits from fewer legs resulting in reduced size, reduced number of parts, simpler modelling as well as smaller lost motion. Compared with existing 2-legged designs with conventional arrangement, the present design has smaller parasitic rotation, which has been proved from the FEA results.

KEYWORDS: Compliant mechanisms, Compactness, Parasitic motion, Stiffness center, Decoupling, Nonlinear modelling;

1 INTRODUCTION

There is an increasing need for designing compact large-range XY parallel flexure motion stages for a variety of applications such as AFM (atomic force microscope) scanning tables for bio-medical applications [1-3]. The XY parallel flexure motion stage is an XY compliant parallel manipulator (CPM) that is composed of a fixed base and a motion stage connected by compliant members actuated by linear actuators indirectly. Its motion stage only translates in the XY plane by the deformation of the compliant members. Compared with its rigid-body counterparts, the XY CPM has plenty of merits such as eliminated backlash and friction, no need for lubrication, reduced wear and noise, high precision up to nano-metric, high payloads, reduced number of parts, more-compact and monolithic configuration [4].

In compliant mechanisms, distributed-compliance is often used for increasing the motion range. However, parasitic motion such as undesired rotation will always accompany its primary translation inherently if no suitable measure is taken, which can adversely affect the positioning/scanning accuracy. For example, a commonly-used parallelogram flexure mechanism produces a transverse primary motion caused by the force acting at the tip of the flexure with the consequence that active rotation compensation is needed to maintain a zero rotation at the tip. In addition, the cross-axis coupling between the X- and Y- axes can introduce the complicated control and measurement uncertainties in the scanning processing [5]. Recent research advances have enabled the desired designs with decoupled configuration and minimised parasitic rotation in XY CPMs. For instance, based on a 4-PP (P: prismatic) kinematically decoupled[1] translational parallel manipulator (TPM) (Figure 1a), both the rotational symmetry [6, 7] and mirror symmetry [6-9] constraints for compliant modules, especially mirror symmetry, were used to produce the kinematostatically decoupled[2] XY

[1] Kinematic decoupling can be classified into two types: complete decoupling and partial decoupling. This paper only concerns the complete kinematic decoupling, which refers to that each independent output motion is controlled by only one input motion.

[2] Kinematostatic decoupling means that one primary output translational displacement is only affected by the actuation force along the same direction, which describes the relationship between the input force and output motion. This decoupling (no absolute) is also called the output-decoupling/minimal cross-axis coupling in CPMs. Kinematostatic coupling may lead to complicated motion control, which is the sufficient condition of kinematic decoupling.

CPMs with other good characteristics such as minimised parasitic rotations and the maximal actuator isolation (minimal input-coupling) [6]. Despite their characteristics, such rotational/mirror symmetry strategies, however, introduce a trade-off between the minimised parasitic motion (due to symmetry) and large size/increased number of parts (due to using 4 legs) of 4-PP XY CPMs compared to the 2-legged (2-PP) XY CPMs according to the 2-PP TPM (Figure 1b). Moreover, the symmetric 4-legged design may cause relatively large lost motion (between the input motion and output motion) due to the fact that the passive P joint connected to one actuated P joint in one leg transfers loads to the rest three leg legs rather than only one leg. In addition, hybrid-compliance modules [10] were used to reduce the parasitic rotation but subject to the fact that lumped-compliance results in small motion range and stress concentration.

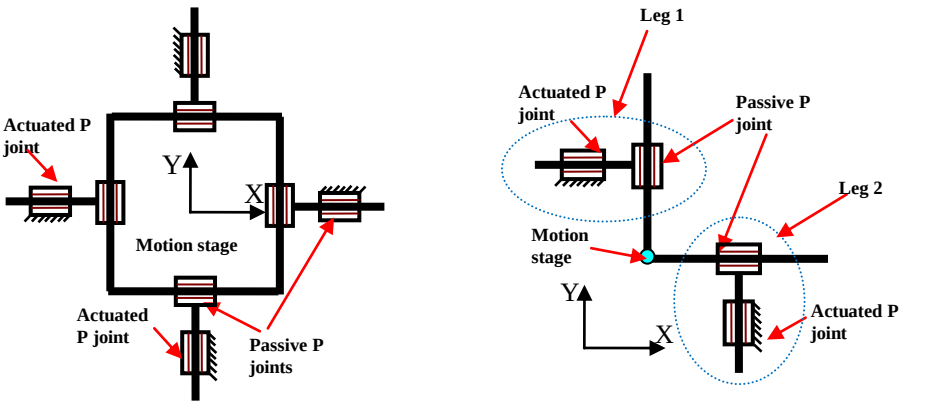

(a) 4-PP kinematically decoupled TPM **(b) 2-PP kinematically decoupled TPM**

Fig. 1 XY parallel manipulators

Moreover, the design of partial stiffness center based was discussed in [6] for a 2-legged XY CPM, which can only well minimise the parasitic rotational yaw if only ONE actuation force is applied. The stiffness center [7, 11] refers to a point through which an actuation force, parallel to the primary motion, is applied on the motion stage of a compliant module to produce the primary translation and minimize any parasitic rotation. The indicated stiffness center of a parallelogram module is shown in Figure 2, which are the symmetric centers of all compliant beams.

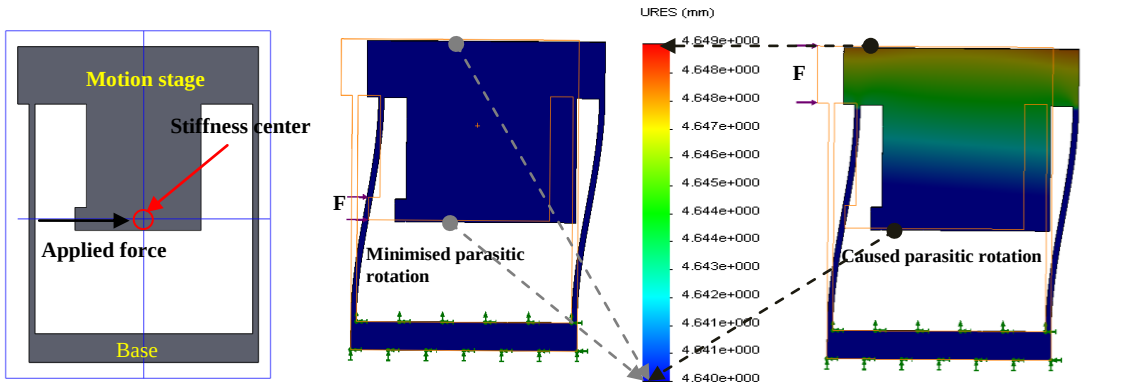

(a) Undeformed configuration **(b) Deformed configuration for applied force acting at the stiffness center** **(c) Deformed configuration for applied force NOT acting at the stiffness center**

Fig. 2 Stiffness center demonstration for a parallelogram module

In order to better reduce the parasitic rotations of multi-DOF (degrees of freedom) translational CPMs and make the configuration more compact, an innovative design approach of full stiffness center based is presented in this paper building on the above advances and a corresponding 2-legged XY CPM is designed, modelled and theoretically analyzed.

The remainder of this paper is organised as follows. Section 2 states the novel design approach of stiffness center based for XY CPMs. In Sec. 3, a compact and decoupled XY CPM with minimised parasitic rotation is proposed and described. Analytical modelling is implemented with comparisons with FEA in Sec. 4. Finally, conclusions are drawn in Sec. 6.

2 DESIGN APPROACH OF STIFFNESS CENTER BASED FOR XY CPMS

2-legged XY CPMs with minimised parasitic rotation and a compact configuration can be designed following the procedure below:

(1) Replace the traditional kinematic joints with appropriate distributed-compliance parallelogram modules based on the configuration of 2-PP kinematically decoupled TPMs (Figure 1b).

(2) Re-arrange the passive compliant modules to make all the stiffness centers, associated with the passive modules, overlap at a same point that all the applied input forces can go through. Therefore, an appropriate embedded arrangement must be performed to integrate all the passive compliant modules together.

(3) Take further measures to make the whole configuration compact, and/or address certain specific requirement.

In Sec. 3, an example monolithic XY CPM will be presented using the above design approach. More examples can be obtained based on the actual needs/applications using the proposed approach similar to the case in Section 3. For example, one can use different actuated compliant P joint and/or increase the beam number (elasticity average) in the compliant parallelogram modules. In addition, a monolithic 2-legged XY CPM with minimised parasitic rotation may be proposed according to the strategy of both partial symmetry and partial stiffness center overlapping (see Appendix A for details). Three types of 2-legged stacked XY CPMs with further reduced size using a two-level strategy will also be discussed in Appendix B to demonstrate diverse applications of the design approach of stiffness center based. It should be noted that the proposed approach to minimise the parasitic rotation can be used to design the 3-legged spatial translational CPMs.

3 DESIGN OF A 2-LEGGED XY CPM WITH STIFFNESS CENTER OVERLAPPING

3.1 DESIGN CONSIDERATIONS

In addition to kinematostatic decoupling and minimised parasitic rotations mentioned in the introduction section, the following design criteria should be considered to obtain a high-performance XY CPM.

1) Material and actuator selections

AL6061-T6 and AL7075-T6 are recommended for precision instruments due to the material's low internal stresses, good strength and phase stability [7]. In this paper, AL6061-T6, with Young's Modules E = 69 Gpa, Yield stress 276 Mpa and Poisson's ratio v = 0.33, is selected for modelling and FEA comparisons owing to its low cost.

It is noted that the millimetre-level motion range requires a large-range linear actuator, which cannot be a PZT actuator. Although amplifiers as actuated compliant P joints can be combined with the PZT actuator to enlarge the motion range [9], adversely, they lead to relatively low off-axis stiffness and augment the minimum incremental motion of the actuators. Thus, one needs to choose the linear *Voice Coil* actuator [12] for millimetre-level actuation range. This linear actuator has merits such as large-range nanopositioning (the large range of motion and high nanometric resolution), linear model, and force-control along with hysteresis-free, frictionless and cog-free motion. Due to the nature that heat dissipates from the coil in the actuator, thus the magnet along with the back iron is connected to the input stage of the 2-legged XY CPM to improve the thermal stability [13].

2) Monolithic design and fabrication

In order to avoid the negative effects such as assembly error, increased number of parts, reduced stiffness (by about 30% by bolted joints) and increased cost, the monolithic design is always desired.

The well-known CNC multi-axis milling machining is extensively used to fabricate precise parts in industry. However, there are three main issues for the compliant mechanism manufacture. One is that the thickness of the in-depth features must be not larger than the driller length. The second is that the in-plane small thickness of the features is limited by the nature of the contact machining producing loading to the thin features, which has to be verified by repeated experiments by an experienced technician. The third is that the gap size between two adjacent features is largely constrained by the diameter of the driller. In addition, the milling machining is also time-consuming for fabricating a deep feature due to the nature of the machining.

However, the monolithic XY CPM can be directly fabricated using wire electrical discharge machining (wire EDM). Dimensional tolerances better than 12 microns in plane are easily achievable due to the non-contact machining, parallelism and perpendicularity of the machined feature can be tightly controlled [7]. Also, with wire EDM, the in-depth feature thickness of the plate being machined is not a concern. But the EDM process requires a fairly significant amount of set-up works and is generally expensive.

3) Actuator isolation design

Due to the fact that linear actuators (such as PZT and Voice Coil) and the input linear displacement sensors (such as optical linear encoder) cannot tolerate the transverse motion/load, so the actuated compliant P joint should have a *mirror-symmetric form* with regard to the actuation axis through using two identical compliant P joints in a parallel form [8].

4) Large-range motion design

The XY CPM to be proposed should be able to generate millimetre-level large range of motion without stress-concentration at a conceptual level rather than reducing the thickness and increasing length of beams. Enlarging the length of beams can make the configuration bulky and reducing the thickness of beams may result in the decrease of stiffness significantly and other issues such as manufacturability. A good recommendation is to use the distributed-compliance and the double parallelogram module (a multi-level strategy involving the secondary stage [7, 11]) to construct the actuated compliant P joints. Especially, the use of the two mirror-symmetric *double* parallelogram modules as the actuated P joint can largely alleviate the significant load-stiffening effect [7] compared to two mirror-symmetry *basic* parallelogram modules. Here, this load-stiffening effect 1) significantly nonlinearly increases the primary motion stiffness resulting in the use of only small motion linear actuators such as PZT actuators, and 2) significantly increases the tensile stress causing the ease of material yield under large range of motion.

5) Good dynamics

From the dynamic equation, it is clear that one may reduce the mass or increase the stiffness to raise the modal frequencies for improving the dynamic performance of the proposed XY CPM (Figure 3).

There are under-constrained secondary stages involved in the actuated compliant P joints in the case of using double parallelogram modules as recommended above, which can undergo free vibration along the unconstrained directions. It can be noted that the resulting XY CPM can behave well under quasi-statical/low speed motion mode, in which the secondary stages do not vibrate uncontrollably. However, if one intends to run the XY CPM in an appreciable speed, a tradeoff has to be made between good characteristics, such as large range of motion achieved through the use of the double parallelogram modules involving the secondary stages, and the uncontrollable vibration mentioned above.

The mounting strategy for the Voice Coil actuator mentioned earlier will add also large mass of the magnet and back iron to the compliant mechanism and result in the low natural frequency issue limiting the bandwidth of the motion system [13].

In order to improve the dynamic performance, we can therefore increase the beam number (elasticity average) only in the actuated compliant P joints to raise the natural frequency with better actuator isolation performance but without affecting the maximal motion range and causing worse lost motion. In addition to the above measures, one may also improve the dynamic performance by using a high-order controller to achieve a high bandwidth greater than the first natural frequency [12].

6) Other considerations

It can be envisaged that the parasitic rotation and cross-axis coupling effects may be further slightly reduced by two methods: 1) increasing the off-axis stiffness of the actuated compliant P joints, and 2) increasing the in-plane thickness of the rigid parts to approach the assumption of their absolute rigidity. The former method can be achieved by a) increasing the number of compliant beams, and/or b) using a different type of actuated compliant P joint with higher off-axis stiffness over the motion range [14]. The latter method will result in a dynamic issue.

3.2 EMBODIMENT OF THE XY CPM

Using the design approach proposed in Sec. 2 with the design criteria considered in Sec 3.1, a novel 2-legged kinematostatically decoupled XY CPM (Figure 3) with minimised parasitic rotation and a compact configuration is obtained by replacing each actuated P joint and each passive P joint in a 2-PP TPM (Figure 1b) with an actuated compliant P joint and a passive compliant P joint, respectively, and making two stiffness center of two passive compliant P joints overlap at the same point.

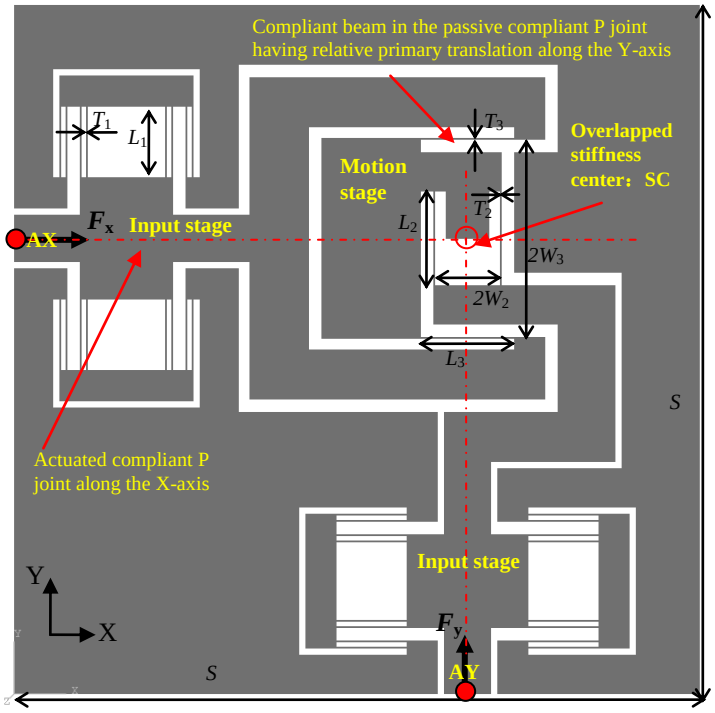

Fig. 3 A 2-PP XY CPM with stiffness center overlapping of two passive P joints

As shown in Figure 3, two actuated compliant P joints are identical and can be actuated by two linear actuators at the input points AX and AY, respectively, each of which is composed of two mirror-symmetry double (four-beam) parallelogram modules to address the issue of large range of

motion and actuator isolation. Each passive compliant P joint is a parallelogram module connected to the motion stage, which has no non-controllable motion mass from the good dynamics point of view. It is noted that two passive compliant P joints may be not identical in order to make embedded arrangement, but the ratios of length (L_2 or L_3) to in-plane thickness (T_2 or T_3) of the beams in both passive compliant P joints are same for producing same primary motion stiffness along each axis.

4 THEORETICAL CHARACTERISTICS ANALYSIS

Under the action of two input forces, F_x and F_y, exerted at two input points, AX and AY, as indicated in Figure 3, the following main static characteristics will be investigated by the analytical modelling and/or FEA results.

1) Relationships between the input force and output displacements. The output displacement is specified at the SC point on the motion range as shown in Figure 3. These relationships can not only reflect the nominal primary motion stiffness (single loading), but also the cross-axis coupling effect, $(Y_{SC}-Y_{SC}|_{Fx=0})/X_{SC}|_{Fy=0}$ or $(X_{SC}-X_{SC}|_{Fy=0})/Y_{SC}|_{Fx=0}$.

2) Parasitic rotation. Parasitic rotation is specified for the rotation of the motion stage, which can be obtained by the displacement difference of any two points on the motion stage.

3) Actuator non-isolation effect (i.e. input coupling effect). Input-coupling is specified for the transverse motion at the two actuation points, AX and AY. Input-coupling effect can be denoted as Y_{AX}/Y_{SC} or X_{AY}/X_{SC}.

4) Input and output motion difference, which can be expressed by $(X_{AX}-X_{SC})/X_{SC}$ or $(Y_{AY}-Y_{SC})/Y_{SC}$.

In addition, the motion range equation is further derived and the geometrical parameters are then determined by specifying the desired motion range.

4.1 ANALYTICAL INPUT-FORCE AND OUTPUT-DISPLACEMENT EQUATIONS

The analytical primary motion stiffness is first estimated in a simplified symbolic form as

$$K = K_a + K_p = \frac{4EUT_1^3}{L_1^3} + \frac{2EUT_2^3}{L_2^3} = \frac{4EUT_1^3}{L_1^3} + \frac{2EUT_3^3}{L_3^3} \tag{1}$$

where $T_2 / L_2 = T_3 / L_3$, which is designated to ensure the same primary stiffness along two axes as mentioned earlier. K is the linear primary translational stiffness of the system along each axis. $K_a = 4EUT_1^3 / L_1^3$, which is the primary stiffness of each actuated compliant P joint obtained based on the linear beam theory without accounting for the negligible load-stiffening effect, and $K_p = 2EUT_2^3 / L_2^3 = 2EUT_3^3 / L_3^3$, which is the primary stiffness of each passive compliant P joint based on the linear beam theory as well. All the geometry symbols' definition can refer to Figure 3.

In order to capture the slight cross-axis coupling under the assumption of eliminated parasitic rotation, we can obtain the following equations based on the relative deformation of the passive P joint (Figure 4):

$$\Delta_1+\Delta_2=0.6\Delta^2/L, \tag{2}$$

$$K_a\Delta_1=K_p\Delta_2 \tag{3}$$

where Equation (2) is the geometric compatibility condition, and Equation (3) is the load-equilibrium condition. In Equation (2), the right-hand term: $0.6\Delta^2/L$ is the introduced parasitic translation associated with the kinematic effect [7] of a parallelogram module with it beam length of L. Δ is primary translation of the passive P joint. Δ_1 is the displacement of the actuated P joint caused by this parasitic translation along the same direction, and Δ_2 is the motion stage displacement caused by this parasitic translation along the same direction.

From Equations (2) ad (3), we can obtain the solution for Δ_1 and Δ_2:

$$\Delta_1 = 0.6\Delta^2(\frac{K_p}{K})L\,, \tag{4}$$

$$\Delta_2 = 0.6\Delta^2(\frac{K_a}{K})L\,. \tag{5}$$

Combining Equations (1), (4) and (5), simple but relatively accurate nonlinear load-displacement equations for the XY CPM can be written to capture nonlinear characteristics as

$$X_{SC} = \frac{F_x}{K} + 0.6(\frac{F_y}{KL_3})^2(\frac{K_a}{K})L_3\,, \tag{5}$$

$$Y_{SC} = \frac{F_y}{K} - 0.6(\frac{F_x}{KL_2})^2(\frac{K_a}{K})L_2\,, \tag{6}$$

$$X_{AX} = \frac{F_x}{K} - 0.6(\frac{F_y}{KL_3})^2(\frac{K_p}{K})L_3\,, \tag{7}$$

$$Y_{AY} = \frac{F_y}{K} + 0.6(\frac{F_x}{KL_2})^2(\frac{K_p}{K})L_2 \tag{8}$$

where X_{SC} and Y_{SC} are the translational displacements of the overlapped stiffness center, SC, on the motion stage along the X- and Y-axes, respectively. X_{AX} and Y_{AY} are the primary translational displacements at the two input points, AX and AY, along the X- and Y-axes, respectively. F_x and F_y are the applied input forces at the two input points along the X- and Y-axes, respectively.

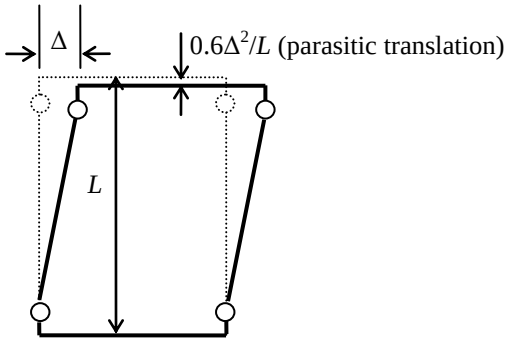

Fig. 4 Passive P joint (parallelogram module) relative deformation

It is noted that the above cross-axis coupling is very small and easily addressed in motion systems via feedback controls. In principle, the stiffness center based approach is capable of largely eliminating the parasitic rotation θ_{SZ}. The linear matrix modelling is also detailed in Appendix C to compare the monolithic 2-legged XY CPM with stiffness center overlapping with the monolithic 2-legged XY CPM without stiffness center overlapping, and further verify the effectiveness of the stiffness center based approach for minimising the parasitic rotation.

4.2 MOTION RANGE AND GEOMETRICAL PARAMETER DETERMINATION

From the initial FEA results, it can be concluded that the bending normal stress in our case is the dominant effects associated with yield compared with other tensile normal stress and/or shear stress effects. Therefore, based on the Von Mises theory and negligible effects of tensile normal stress and shear stress, the motion range of the actuated P joint and two passive P joints should approximately meet the following equations [11]:

$$\Delta_a = \frac{2}{3\eta}\frac{\sigma_s}{E}\frac{{L_1}^2}{T_1}\,, \tag{9}$$

$$\Delta_{p1} = \frac{1}{3\eta}\frac{\sigma_s}{E}\frac{{L_2}^2}{T_2}\,, \tag{10}$$

$$\Delta_{p2} = \frac{1}{3\eta}\frac{\sigma_s}{E}\frac{L_3^{\,2}}{T_3} \tag{11}$$

where η is the safety factor considering actual factors such as stress concentration, which is specified to be 1.35 (or 1.2) for the actuated P joint (or the passive P joint). The motion range of the XY CPM should be the minimal one among Equations (9) to (11).

In order to achieve a motion range of 2 mm along each unidirection (a total motion range of 4mm per bi-direction) and considering the manufacturability for the minimal in-plane thickness, the primary geometrical parameters can therefore be determined as listed in Table 1.

Table 1: Principle geometrical parameters

Length L_1	Length L_2	Length L_3	In-plane thickness T_1	In-plane thickness T_2	In-plane thickness T_3	Spanning size W_2	Spanning size W_3	Out-of-plane thickness U	Overall dimensions $S\times S$
22.5 mm	30 mm	30 mm	0.5 mm	0.5 mm	0.5 mm	10.25 mm	31.75 mm	10 mm	220×220 mm

Substituting the above geometrical parameters into Equation (1), we obtain the system primary stiffness along each axis is 36.68N/mm.

4.3 FEA RESUTLS

Nonlinear FEA was conducted to analyse the performance characteristics of the proposed XY CPM and compared with the proposed analytical models (Equations (5)-(8)). Here, commercial software, Comsol, is selected for FEA using tetrahedral element and finest meshing with other default. The stiffness center on the motion stage is chosen as the reference point for translational displacements of the motion stage.

Figures 5a and 5b illustrate two cases of large-deformation using FEA. One is the translation along the Y-axis, and the other is the translations along both axes.

The primary motion along each axis is shown in Figures 6a and 6b. The analytical results have a very good agreement with the FEA results with the maximal differences of 1.19% and 1.74% for the X- and Y-displacements, respectively.

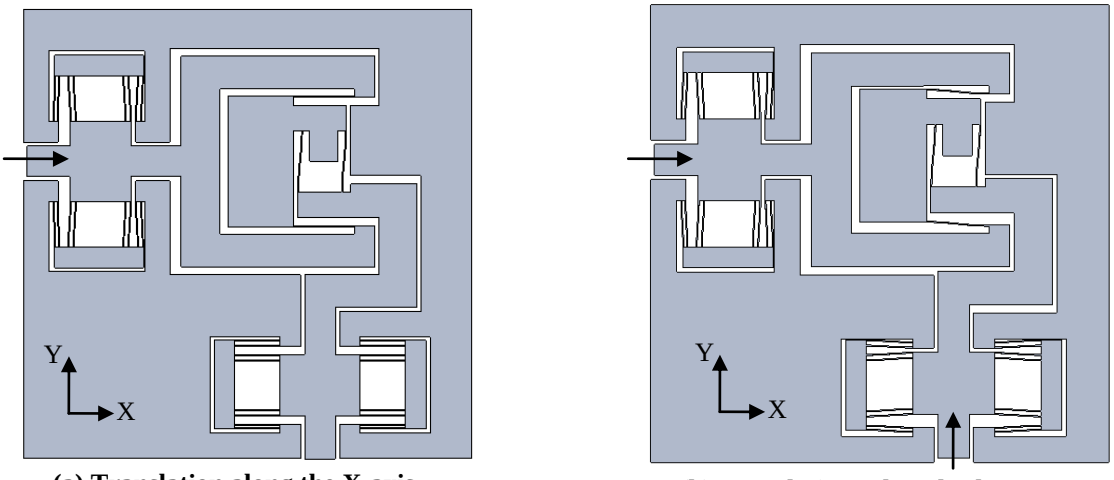

(a) Translation along the X-axis **(b) Translations along both axes**

Fig. 5 FEA deformation demonstration

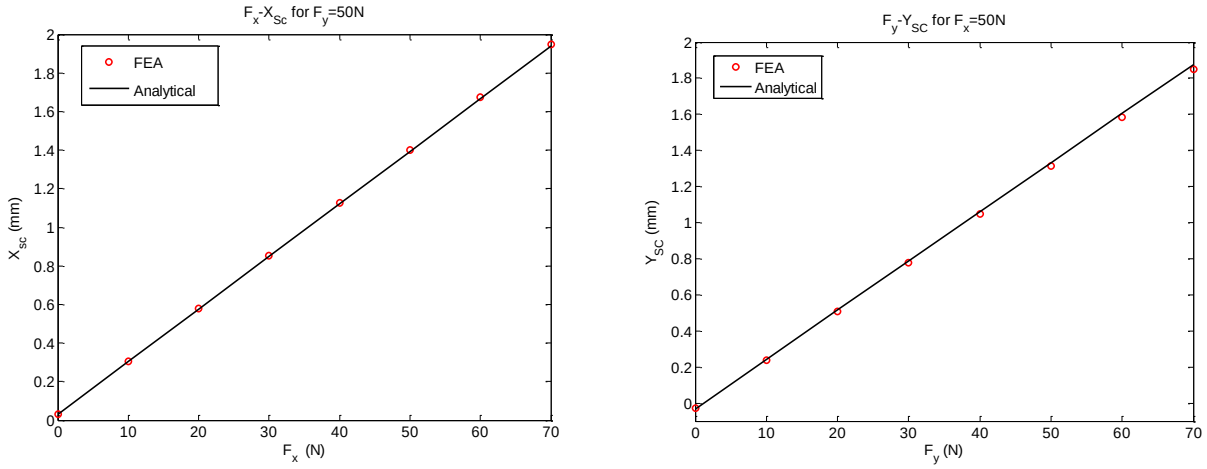

(a) Primary motion along the X-axis **(b) Primary motion along the Y-axis**

Fig. 6 Primary motion along each axis

Figure 7 illustrates that the cross-axis coupling effects obtained from both the analytical model and the FEA results have an acceptable difference. From Figures 7a and 7b, it is shown that the maximal $|(Y_{SC}-Y_{SC}|_{Fx=0})/X_{SC}|_{Fy=0}|$ for the FEA results (or the analytical results) is 5.73% (or 4.41%) and the maximal $|(X_{SC}-X_{SC}|_{Fy=0})/Y_{SC}|_{Fx=0}|$ for the FEA results (or the analytical results) is 5.57% (or 4.41%).

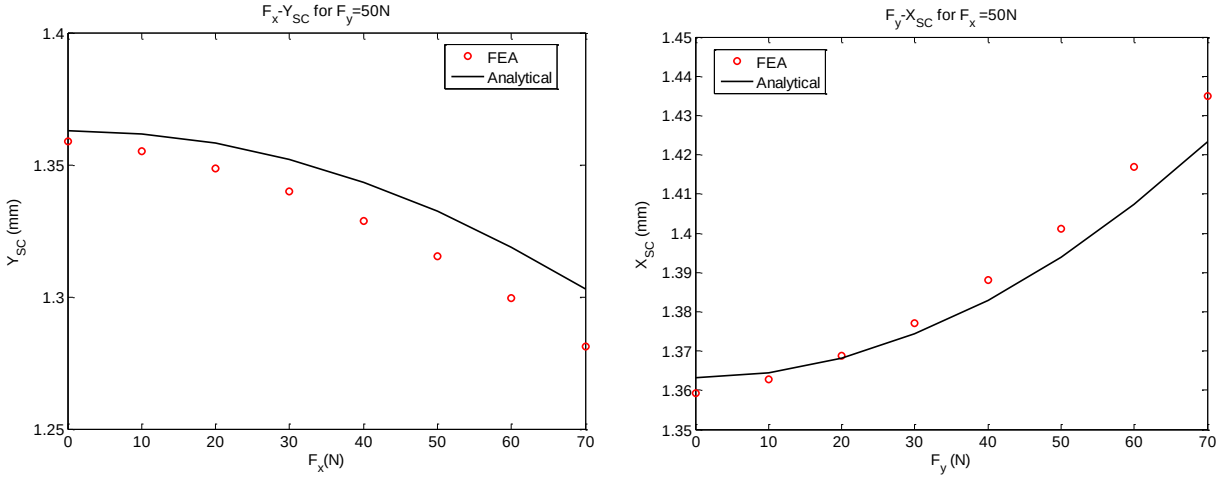

(a) Motion along the Y-axis **(b) Motion along the X-axis**

Fig. 7 Cross-axis coupling effect

The parasitic rotation results obtained from FEA for single loading and two-axis loading are shown in Figure 8. For the XY CPM with stiffness center overlapping, the parasitic rotation caused by the single-axis load F_x is less than 4.0×10^{-6} rad in the magnitude (Figure 8a), and the one caused by the single-axis load F_y is better than 1.5×10^{-5} rad in the magnitude (Figure 8b), which are very close to the analytical results of zero. Moreover, the parasitic rotation caused by the two-axis loads (F_x and F_y=50N) is less than 4.9×10^{-5} rad in the magnitude (Figure 8c), and the one caused by the two-axis loads (F_y and F_x=50N) is lower than 6.2×10^{-5} rad in the magnitude (Figure 8d). As shown in Figures 8a, 8b, 8c, 8d, the stiffness center overlapping strategy works very well to minimise the parasitic rotation in comparison with the conventional arrangement without stiffness center overlapping (Figure C.1), especially for the single-loading case.

Note that the parasitic rotation and the cross-axis coupling results obtained from the FEA model above are larger than those obtained from the analytical model, which may result from the following two aspects: a) all parts are more reasonably considered as elastic bodies in FEA; (b) these characteristics are very small and the FEA model may have relatively large inaccuracy in dealing with very small deformation or displacements.

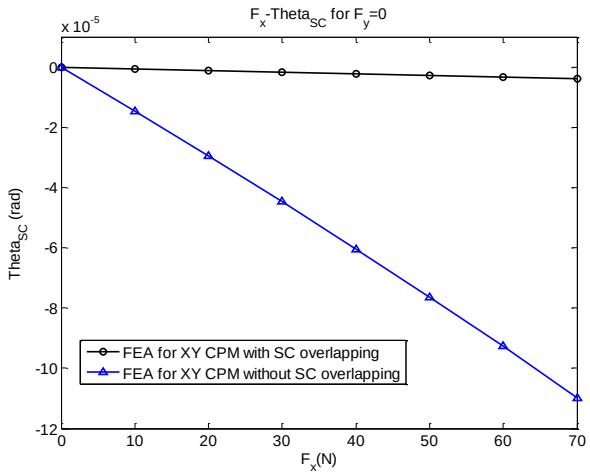

(a) Single-axis loading by F_x

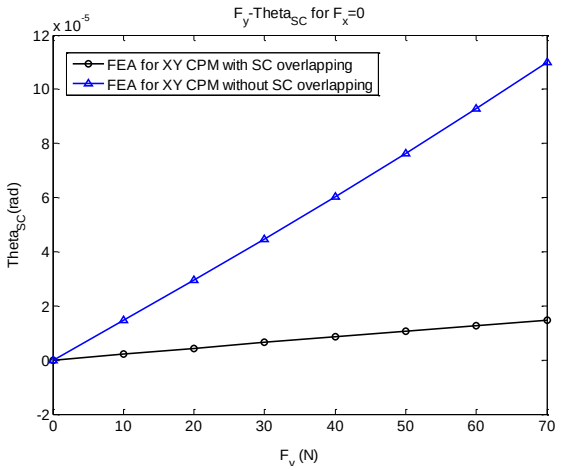

(b) Single-axis loading by F_y

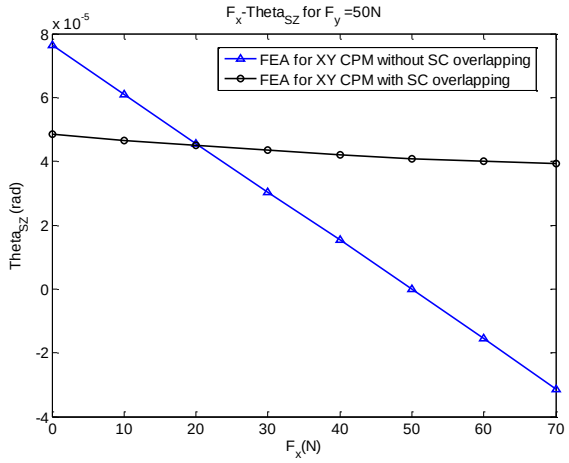

(c) Two-axis loading (F_x and F_y=50N)

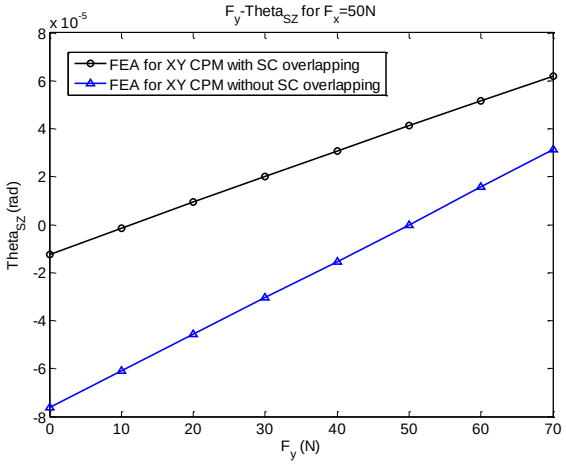

(d) Two-axis loading (F_y and F_x=50N)

Fig. 8 Parasitic rotation results from FEA for two types of XY CPMs

Figure 9 shows that the absolute value of the input and out motion difference, $|(X_{AX}-X_{SC})/X_{SC}|$ (Figure 9a) or $|(Y_{AY}-Y_{SC})/Y_{SC}|$ (Figure 9b) decreases with the increase of the force along the same direction. The maximal motion difference in magnitude is about 12% in Figure 9a or 15% in Figure 9b. It is noted that both the analytical results comply with the FEA results very well.

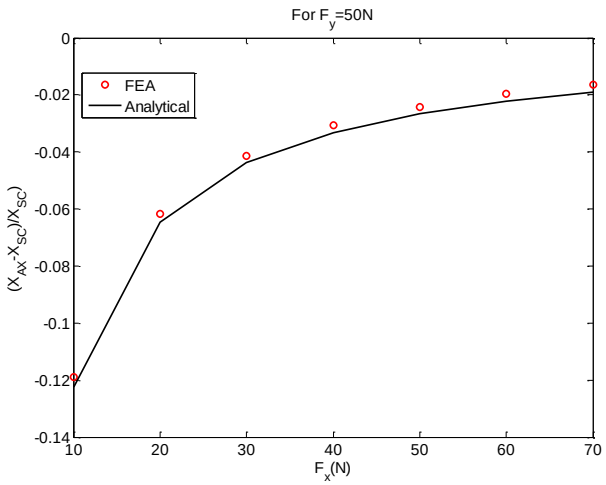

(a) Difference in the X-direction

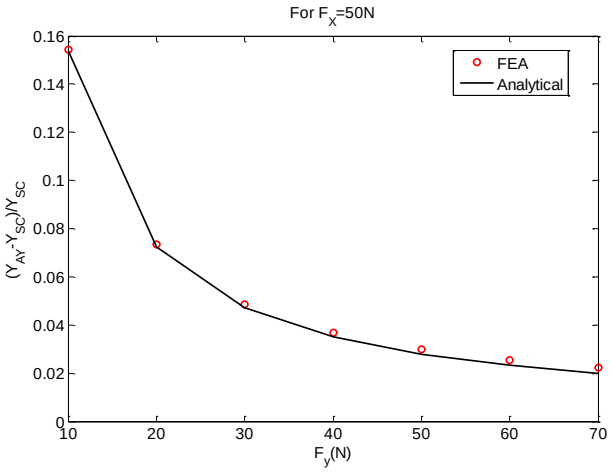

(b) Difference in the Y-direction

Fig. 9 Input and output motion difference

.

Actuator non-isolation analysis is implemented by FEA in Figure 10. It can be found that the actuator transverse motion percentage, Y_{AX}/Y_{SC} or X_{AY}/X_{SC}, is lower than 0.1%, which is a negligible influence on the linear actuator function. Figure 10 also implies that the off-axis translational stiffness of the actuated P joint drops significantly with the increase of the motion range, which is its disadvantage.

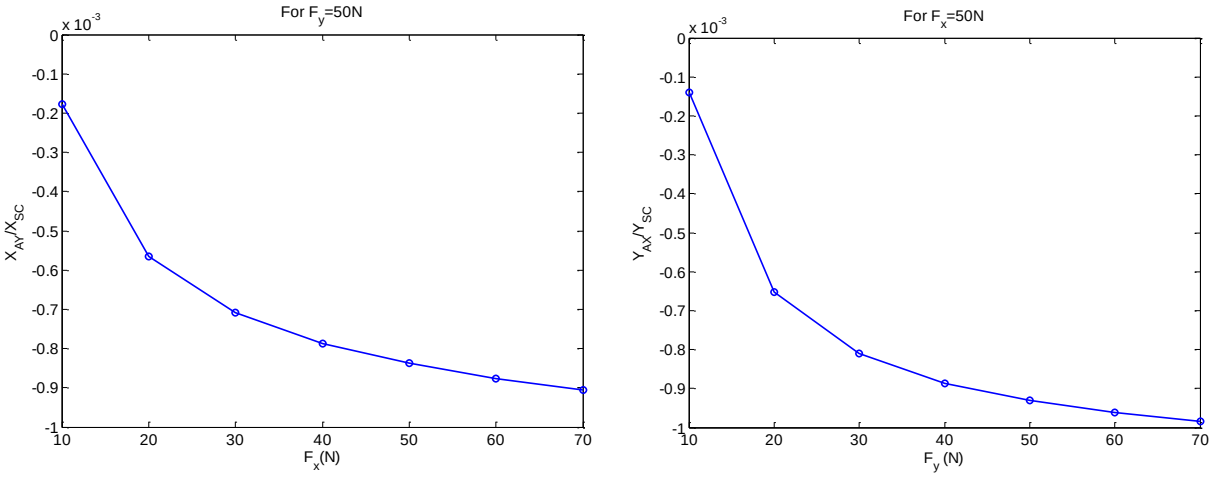

(a) Analysis for the X-axis **(b) Analysis for the Y-axis**

Fig. 10 Actuator non-isolation analysis using FEA

5 CONCLUSIONS

A monolithic compact and decoupled XY CPM with minimised parasitic rotation has been proposed using the approach of stiffness center based, and modelled with comparisons with FEA. This novel design presents an alternative idea to reduce the parasitic rotation using fewer legs. In addition to the performance characteristics including compact configuration, approximately kinematostatic decoupling and minimised parasitic rotation, the proposed XY CPM also has a millimetre-level motion range (4 mm per bi-direction), and can well deal with the issue of actuator isolation.

In comparison with the emerging monolithic XY CPMs obtained from the configuration of 4-PP kinematically decoupled TPM, apparently, the present XY CPM mainly has a smaller size, reduced number of parts, simpler modelling as well as smaller lost motion due to the use of only two legs. Compared with existing monolithic 2-legged designs with conventional arrangement (without stiffness center overlapping), the present design has smaller parasitic rotation. In addition, the two-legged stacked XY CPMs with further reduced size are also presented in this paper.

The optimization considering a balance between the motion mass of the system (and therefore dynamic performance) and the geometrical parameters of the assumed rigid parts to further reduce the parasitic rotation and cross-axis coupling, and the experiment verification deserve investigation in the future.

ACKNOWLEDGEMENT

The author would like to acknowledge Mr. Haiyang Li for his work in creating the CAD models (Figures B.1, B.2 and C.1). Special acknowledgement goes to Dr. Qiaoling Meng for her contribution in the nonlinear FEA. The valuable comments from the two anonymous reviewers are greatly appreciated.

REFERENCES

1 **Kim D, Lee DY** and **Gweon DG.** A New Nano-Accuracy AFM System for Minimizing Abbe Errors and the Evaluation of Its Measuring Uncertainty. *Ultramicroscopy*, 2007, **107**(4-5), 322–328.

2 **Schitter G, Thurner PJ** and **Hansma PK.** Design and Input-Shaping Control of a Novel

Scanner for High-Speed Atomic Force Microscopy. *Mechatronics*, 2008, **18**(5-6), 282–288.
3 **Werner C, Rosielle PCJN** and **Steinbuch M.** Design of a Long Stroke Translation Stage for AFM. *International Journal Machine Tools and Manufacture*, 2010, **50**(2), 183–190.
4 **Howell LL.** *Compliant Mechanisms*. New York: Wiley, 2001.
5 **Yong YK** and **Liu KX.** Reducing Cross-Coupling in a Compliant XY Nanopositioner for Fast and Accurate Raster Scanning. *IEEE Transactions on Control Systems and Technology*, 2010, **18**(5), 1172–1179.
6 **Awtar S** and **Slocum AH.** Constraint-Based Design of Parallel Kinematic XY Flexure Mechanisms. *Journal of Mechanical Design*, 2007, **129**(8), 816–830.
7 **Awtar S.** *Analysis and Synthesis of Planer Kinematic XY Mechanisms*. Sc.D. thesis, Massachusetts Institute of Technology, Cambridge, MA, 2004.
8 **Choi KB** and **Kim DH.** Monolithic Parallel Linear Compliant Mechanism for Two Axes Ultra Precision Linear Motion. *Review of Scientific Instruments*, 2006, **77**(6): 065106.
9 **Li Y** and **Xu Q.** Design and Analysis of a Totally Decoupled Flexure-Based XY Parallel Micromanipulator. *IEEE Transactions on Robotics*, 2009, **25**(3): 645 – 657.
10 **Polit S** and **Dong JY**. Design of High-Bandwidth High-Precision Flexure-Based Nanopositioning Modules. *Journal of Manufacturing Systems*, 2009, **28**:71–77.
11 **Hao G**. *Creative Design and Modelling of Large-Range Translational Compliant Parallel Manipulators*. PhD Thesis, Heriot-Watt University, Edinburgh, UK, 2011.
12 **Awtar S** and **Parmar G**. Design of a Large Range XY Nanopostioning System. In: *the ASME 2010 International Design Engineering Technical Conferences & Computers and Information in Engineering Conference*, Montreal, Quebec, Canada, August 15-18, 2010, paper no. DETC2010-28185. New York: ASME.
13 **Hiemstra DB, Parmar G,** and **Awtar S.** Performance Tradeoffs Posed by Moving Magnet Actuators in Flexure-Based Nanopositioning. IEEE/ASME Transactions on Mechatronics. In Press.
14 **Olfatnia M**, **Sood S**, **Gorman JJ**, and **Awtar S**. Large Stroke Electrostatic Comb-Drive Actuators Enabled by a Novel Flexure Mechanism. Journal of Microelectromechanical Systems, 2013, **22**(2):483-494
15 **Hao G** and **Kong X**. Novel XY Compliant Parallel Manipulators for Large Translation with Enhanced Out-of-Plane Stiffness. *Journal of Mechanical Design*, 2012, **134**: 061009.
16 **Hao G** and **Kong X**. Design and Modelling of a Large-Range Modular XYZ Compliant Parallel Manipulators Using Identical Spatial Modules. *Journal of Mechanisms and Robotics*, 2012, **4**: 021009.

APPENDIX A: A 3-Legged XY CPM

Figure A.1 shows a 3-legged (3-PP) XY CPM with minimised parasitic rotation based on the strategy of partial symmetry and partial stiffness center overlapping. It is composed of two types of parallelogram flexure modules with identical beams to produce approximate equal primary motion stiffness along each axis. Note that the applied force along the Y-axis passes through the center of stiffness of the passive parallelogram module having primary translation along the Y-axis.

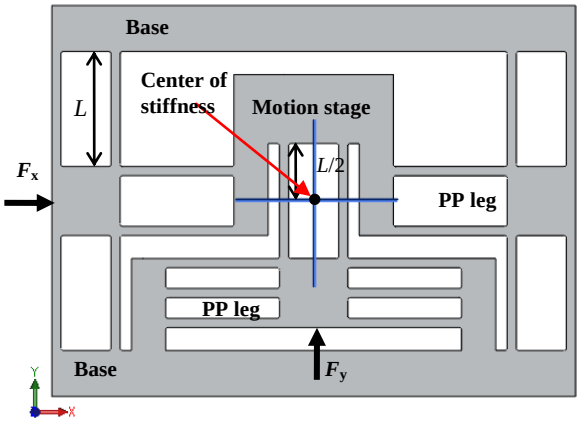

Fig. A.1 A 3-legged XY CPM with minimised parasitic rotation

APPENDIX B: 2-Legged Stacked XY CPMs with Further Reduced Size

Three types of 2-legged stacked XY CPMs with further reduced size are shown in this section (Figures B.1, B.2 and B.3). The stiffness centers of the two passive P joints overlap at the same point for reducing the parasitic rotations. Two identical legs are arranged in two levels with the motion stage connecting two levels.

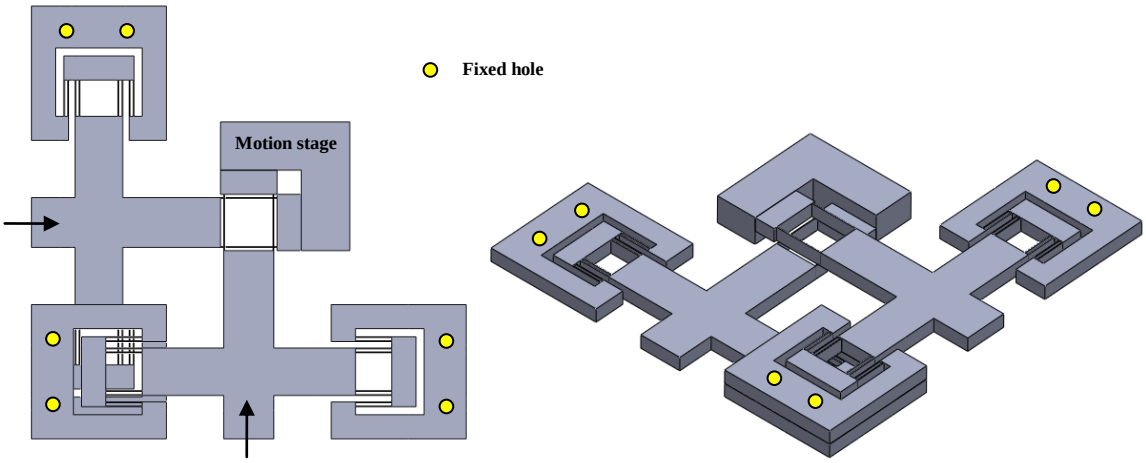

Fig. B.1 Two-legged stacked XY CPM design I: basic parallelogram module as passive P joint

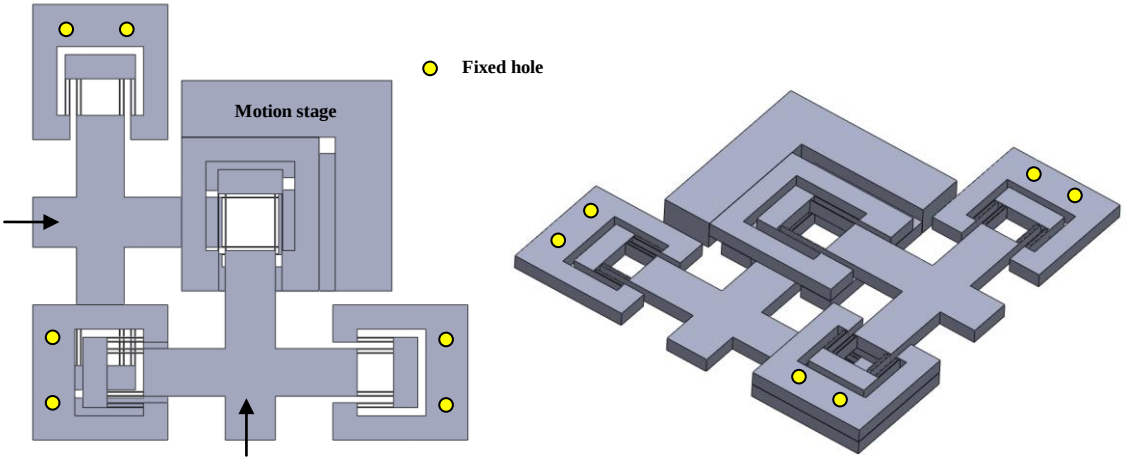

Fig. B.2 Two-legged stacked XY CPM design II: double parallelogram module as passive P joint

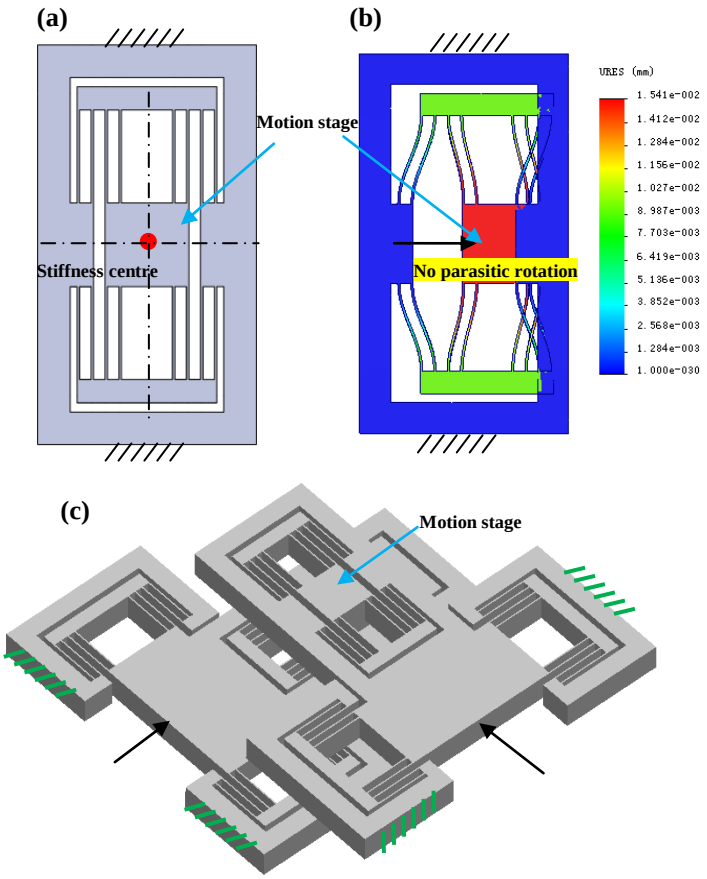

Fig. B.3 Two-legged stacked XY CPM design III using two double parallelogram modules in mirror symmetry as passive P joint: (a) new passive P joint before deformation; (b) deformed configuration of new passive P joint for an applied force acting at the stiffness centre; (c) XY CPM

APPENDIX C: Linear Matrix Modelling

In this section, linear matrix modelling [15, 16] is implemented under small deformation assumptions for Euler-Bernoulli beams in order to the 2-legged XY CPM with minimised parasitic rotation (Figure 3) and the 2-legged XY CPM with conventional arrangement [10] (one example is shown in Figure C.1). The compliance matrix of the latter one will be firstly investigated.

Since the 2-legged XY CPM (Figure C.1) is composed of two identical legs, the focus is on deriving the stiffness and compliance matrices of Leg 1 (along the X-direction). The stiffness and compliance matrices for Leg 2 can be obtained by appropriate coordinate transformation accordingly.

For a passive compliant parallelogram module for loads and displacements both defined at the center of the bottom-plane of its own motion stage, with the spanning parameter of *2W*, its stiffness matrix is obtained as follows:

$$\mathbf{K}_{\mathrm{pm}} = \sum_{i=0}^{2} \mathbf{D}_i^{\mathrm{T}} \mathbf{K} \mathbf{D}_i \tag{C.1}$$

where

$$\mathbf{D}_i = \begin{bmatrix} 1 & 0 & -Y_i' \\ 0 & 1 & X_i' \\ 0 & 0 & 1 \end{bmatrix} \text{ and } \mathbf{K} = \begin{bmatrix} \frac{ET^2}{L} & 0 & 0 \\ 0 & \frac{12EI}{L^3} & -\frac{6EI}{L^2} \\ 0 & -\frac{6EI}{L^2} & \frac{4EI}{L} \end{bmatrix}.$$

Herein, $X_1'=0$ and $Y_1'=W$; $X_2'=0$ and $Y_2'=-W$. E denotes the Young's modulus, and $I=UT^3/12$ denotes the second moment of the cross-sectional area of the compliant beams.

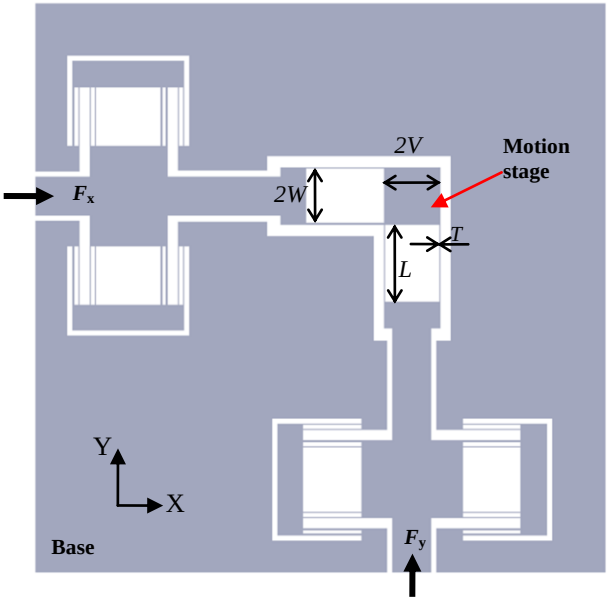

Fig. C.1 A 2-legged XY CPM with conventional arrangement

Thus, the compliance matrix of the passive compliant parallelogram module for loads and displacements both defined at the center of the square motion stage of the XY CPM as

$$\mathbf{C}_{\text{mc}} = \mathbf{J}_{\text{pm}}\mathbf{K}_{\text{pm}}^{-1}\mathbf{J}_{\text{pm}}^{\text{T}} \tag{C.2}$$

where

$$\mathbf{J}_{\text{pm}} = \begin{bmatrix} 1 & 0 & 0 \\ 0 & 1 & V \\ 0 & 0 & 1 \end{bmatrix},$$

which is a transformation matrix obtained based on $\mathbf{D}_i$ in Equation (C.1). $2V$ is the side length of the square motion stage.

Because the primary translational stiffness of the passive parallelogram module is negligible compared to the off-axis stiffness of the actuated compliant P joint, assume that the actuated compliant P joint in Leg 1 has a following simplified compliance matrix

$$\mathbf{C}_{\text{a}} = \begin{bmatrix} C_{\text{a}}, \mathbf{0}_{1\times 2} \\ \mathbf{0}_{2\times 1}, \mathbf{0}_{2\times 2} \end{bmatrix}_{3\times 3} \tag{C.3}$$

where C_{a} represents the primary compliance of the actuated compliant P joint, and $\mathbf{0}_{2\times 2}$ represents a 2×2 zero matrix.

Based on Equations (C.2) and (C.3), the stiffness matrix of Leg 1 for the loads and displacements both defined at the center of the motion stage is

$$\mathbf{K}_{\text{leg1}} = (\mathbf{C}_{\text{a}} + \mathbf{C}_{\text{mc}})^{-1}. \tag{C.4}$$

Using Equation (C.4), the stiffness matrix of the XY CPM for the loads and displacements both defined at the motion stage center can be derived as

$$\mathbf{K}_{\text{cpm}} = \mathbf{K}_{\text{leg1}} + \mathbf{R}_{\text{leg2}}\mathbf{K}_{\text{leg1}}\mathbf{R}_{\text{leg2}}^{-1} \tag{C.5}$$

where

$$\mathbf{R}_{\text{leg2}} = \begin{bmatrix} \cos(\pi/2) & -\sin(\pi/2) & 0 \\ \sin(\pi/2) & \cos(\pi/2) & 0 \\ 0 & 0 & 1 \end{bmatrix}.$$

Accordingly, the compliance matrix for the XY CPM is obtained as

$$\mathbf{C}_{\text{cpm}} = \mathbf{K}_{\text{cpm}}^{-1}. \tag{C.6}$$

Similar to the above modelling for the 2-legged XY CPM with conventional arrangement, one can easily to obtain the compliance matrix of the 2-legged XY CPM with minimised parasitic rotation (Figure 3) as

$$\mathbf{C}_{\text{cpm-sc}} = [\mathbf{R}_{\text{leg1}}(\mathbf{C}_{\text{a}} + \mathbf{C}_{\text{sc1}})^{-1}\mathbf{R}_{\text{leg1}}^{-1} + \mathbf{R}_{\text{leg2}}(\mathbf{C}_{\text{a}} + \mathbf{C}_{\text{sc2}})^{-1}\mathbf{R}_{\text{leg2}}^{-1}]^{-1} \tag{C.7}$$

where

$$\mathbf{R}_{\text{leg1}} = \begin{bmatrix} \cos(\pi) & -\sin(\pi) & 0 \\ \sin(\pi) & \cos(\pi) & 0 \\ 0 & 0 & 1 \end{bmatrix}, \mathbf{C}_{\text{sc1}} = \mathbf{J}_{\text{pm1}}\mathbf{K}_{\text{pm1}}^{-1}\mathbf{J}_{\text{pm1}}^{\text{T}} \text{ and } \mathbf{C}_{\text{sc2}} = \mathbf{J}_{\text{pm2}}\mathbf{K}_{\text{pm2}}^{-1}\mathbf{J}_{\text{pm2}}^{\text{T}}.$$

The other matrices in Equation (C.7) have the same definition as above.

Further, the above $\mathbf{J}_{\text{pm1}}$, $\mathbf{J}_{\text{pm2}}$, $\mathbf{K}_{\text{pm1}}$, and $\mathbf{K}_{\text{pm2}}$ can be expressed as

$$\mathbf{J}_{\text{pm1}} = \begin{bmatrix} 1 & 0 & 0 \\ 0 & 1 & -L_3/2 \\ 0 & 0 & 1 \end{bmatrix}, \mathbf{J}_{\text{pm2}} = \begin{bmatrix} 1 & 0 & 0 \\ 0 & 1 & -L_2/2 \\ 0 & 0 & 1 \end{bmatrix}; \mathbf{K}_{\text{pm1}} = \sum_{i=0}^{2} \mathbf{D}_{1i}^{\text{T}}\mathbf{K}_1\mathbf{D}_{1i}, \mathbf{K}_{\text{pm2}} = \sum_{i=0}^{2} \mathbf{D}_{2i}^{\text{T}}\mathbf{K}_2\mathbf{D}_{2i} \tag{C.8}$$

where

$$\mathbf{D}_{11} = \begin{bmatrix} 1 & 0 & -W_3 \\ 0 & 1 & 0 \\ 0 & 0 & 1 \end{bmatrix}, \mathbf{D}_{12} = \begin{bmatrix} 1 & 0 & W_3 \\ 0 & 1 & 0 \\ 0 & 0 & 1 \end{bmatrix}; \mathbf{D}_{21} = \begin{bmatrix} 1 & 0 & -W_2 \\ 0 & 1 & 0 \\ 0 & 0 & 1 \end{bmatrix}, \mathbf{D}_{22} = \begin{bmatrix} 1 & 0 & W_2 \\ 0 & 1 & 0 \\ 0 & 0 & 1 \end{bmatrix};$$

$$\mathbf{K}_1 = \begin{bmatrix} \frac{ET_3^2}{L_3} & 0 & 0 \\ 0 & \frac{12E}{L_3^3}\left(\frac{UT_3^3}{12}\right) & -\frac{6E}{L_3^2}\left(\frac{UT_3^3}{12}\right) \\ 0 & -\frac{6E}{L_3^2}\left(\frac{UT_3^3}{12}\right) & \frac{4E}{L_3}\left(\frac{UT_3^3}{12}\right) \end{bmatrix}, \mathbf{K}_2 = \begin{bmatrix} \frac{ET_2^2}{L_2} & 0 & 0 \\ 0 & \frac{12E}{L_2^3}\left(\frac{UT_2^3}{12}\right) & -\frac{6E}{L_2^2}\left(\frac{UT_2^3}{12}\right) \\ 0 & -\frac{6E}{L_2^2}\left(\frac{UT_2^3}{12}\right) & \frac{4E}{L_2}\left(\frac{UT_2^3}{12}\right) \end{bmatrix}.$$

As an example, the following parameter values are specified: $L=L_2=L_3=30$ mm, $T=T_2=T_3=0.5$ mm, $V=W=W_2=10.25$mm, $E=69$ GPa, and other geometrical parameters remains the same as those in Table 1.

From Equation (1), it is known that $C_{\text{a}} = 1/30.29\,(\text{mm/N})$. Substituting the above values into Equations (C.6) and (C.7), yields

$$\mathbf{C}_{\text{cpm}} = 1\times10^{-3}\times \begin{bmatrix} 27.9349\,\text{mm/N} & 0.0810\,\text{mm/N} & 0.0180\,\text{N}^{-1} \\ 0.0810\,\text{mm/N} & 27.9349\,\text{mm/N} & 0.0180\,\text{N}^{-1} \\ 0.0180\,\text{rad/N} & 0.0180\,\text{rad/N} & 0.0040\,\text{rad/(Nmm)} \end{bmatrix}, \tag{C. 9}$$

$$\mathbf{C}_{\text{cpm-sc}} = 1\times10^{-3}\times\begin{bmatrix} 2.7935\,\text{mm/N} & 0 & 0 \\ 0 & 2.7935\,\text{mm/N} & 0 \\ 0 & 0 & 0.0004\,\text{rad/(Nmm)} \end{bmatrix}. \quad \text{(C. 10)}$$

Equation (C.9) shows that the 2-legged XY CPM in Figure C.1 is not completely kinematostatically decoupled, and has the inherent parasitic rotation under the action of only actuation forces because the left corner 2×2 sub-matrix is not a zero matrix. It is shown that the same actuation force produces larger rotations if W reduces.

Equation (C.10) shows a diagonal compliance matrix. This implies that the 2-legged XY CPM in Figure 3 is kinematostatically decoupled, and has a zero instantaneous parasitic rotation under the action of only actuation forces. It is noted that the actuation forces do not produce any rotation if the spanning geometry size (W_2 or W_3) decreases or the beam thickness increases. Therefore, the stiffness center based approach is proved again to be effective to minimise the parasitic rotation.